Hydrol. Earth Syst. Sci. Discuss., 10, 9057–9103, 2013
www.hydrol-earth-syst-sci-discuss.net/10/9057/2013/
doi:10.5194/hessd-10-9057-2013

Hydrology and Earth System Sciences
Open Access
Discussions

Integrating ASCAT surface soil moisture and GEOV1 leaf area index into the SURFEX modelling platform: a land data assimilation application over France

A. L. Barbu, J.-C. Calvet, J.-F. Mahfouf, and S. Lafont

CNRM-GAME, UMR3589, Météo France, CNRS, Toulouse, France

Received: 21 May 2013 – Accepted: 26 June 2013 – Published: 11 July 2013

Correspondence to: J.-C. Calvet (jean-christophe.calvet@meteo.fr)

Published by Copernicus Publications on behalf of the European Geosciences Union.

Abstract

The land monitoring service of the European Copernicus programme has developed a set of satellite-based biogeophysical products, including surface soil moisture (SSM) and leaf area index (LAI). This study investigates the impact of joint assimilation of remotely sensed SSM derived from ASCAT backscatter data and the GEOV1 satellite-based LAI into the ISBA-A-gs land surface model within the SURFEX modelling platform of Meteo-France. The ASCAT data were bias corrected with respect to the model climatology by using a seasonal-based CDF (Cumulative Distribution Function) matching technique. A multivariate multi-scale land data assimilation system (LDAS) based on the Extended Kalman Filter (EKF) is used for monitoring the soil moisture, terrestrial vegetation, surface carbon and energy fluxes across the France domain at a spatial resolution of 8 km. Each model grid box is divided in a number of land covers, each having its own set of prognostic variables. The filter algorithm is designed to provide a distinct analysis for each land cover while using one observation per grid box. The updated values are aggregated by computing a weighted average.

In this study, it is demonstrated that the assimilation scheme works effectively within the ISBA-A-gs model over a four-year period (2008–2011). The EKF is able to extract useful information from the data signal at the grid scale and to distribute the root-zone soil moisture and LAI increments among the mosaic structure of the model. The impact of the assimilation on the vegetation phenology and on the water and carbon fluxes varies from one season to another. The spring drought of 2011 is an interesting case study showing the potential of the assimilation to improve drought monitoring. A comparison between simulated and in situ soil moisture gathered at the twelve SMOS-MANIA stations shows improved anomaly correlations for eight stations.

HESSD

10, 9057–9103, 2013

1 Introduction

Monitoring the seasonal and interannual variability of the water and carbon cycles over land is needed for many applications, including hydrological and climate studies. The possibility of improving the performance of land surface models (LSM) using remotely sensed observations is a field of active research. The mechanism of integrating observations, in a statistically optimal way, into a numerical model is called data assimilation. The latter permits improving the representation of the dynamical behavior of a biogeophysical system. Land data assimilation systems (LDAS) are needed to integrate satellite data providing information about land state variables such as the surface soil moisture (SSM) and leaf area index (LAI) into LSM.

Soil moisture is a key factor controlling both the water and energy cycles (through its impact on the fluxes partitioning at the surface). In addition, it is linked to the carbon cycle through the coupling between plant transpiration and photosynthesis. A number of studies have discussed the importance of soil moisture in the description of the carbon cycle whose connexions with the hydrological cycle are largely unknown (van der Molen et al., 2011). Moreover, in the context of the global warming trend, the soil water availability may play a role on ecosystem carbon fluxes far more important than considered until now (Reichstein et al., 2007). Assimilating remotely sensed SSM data into a LSM has been proved to be effective in estimating deeper soil moisture in a large number of papers in various contexts, as hydrology (Houser et al., 1998; Reichle et al., 2002; Draper et al., 2011), numerical weather prediction (NWP) (Mahfouf et al., 2010; Dharssi et al., 2011; De Rosnay et al., 2012) or agricultural studies (Bolten and Crow, 2012).

Also, LAI impacts the exchanges of water vapour and CO_2 between the vegetation canopy and the atmosphere. A number of studies (Jarlan et al., 2008; Gu et al., 2006; Demarty et al., 2007) have shown the potential of assimilating LAI observations to correct vegetation model states.

HESSD
10, 9057–9103, 2013

Recognizing the importance of better exploiting the close link between soil moisture and vegetation variables, efforts were made to implement data assimilation schemes into complex models such as coupled hydrological and crop models or physiologically-based LSM. The possibility of combining these two data streams within such models has been explored in several data assimilation applications either by setting observing system simulation experiments (Pauwels et al., 2007; Nearing et al., 2012) or in real environments (Sabater et al., 2008; Barbu et al., 2011). The complementary nature of different types of data has been highlighted also in Kaminski et al. (2012) and Kato et al. (2013) by considering various pairs of observations (fraction of absorbed photosynthetically active radiation fAPAR and atmospheric CO_2 or fAPAR and latent heat fluxes, respectively). They pointed out the necessity of considering the assimilation of multiple data streams as a more appropriate approach to the complexity of physical phenomena and more robust for the identification of model and data biases.

This study is placed in the context of multivariate multi-scale data assimilation (MVMS DA) within an externalized surface (SURFEX) modelling platform of Meteo-France, after a nomenclature used in Montzka et al. (2012). Several types of data at various spatial scales may be incorporated into a LSM using the Extended Kalman Filter (EKF) (Mahfouf et al., 2009). Different versions of the EKF technique were used in various studies in order to assimilate either soil moisture (Draper et al., 2009), LAI (Jarlan et al., 2008), or both LAI and soil moisture (Sabater et al., 2008; Barbu et al., 2011).

This study is an extension of a previous work by Barbu et al. (2011) where the joint assimilation of ground-based soil moisture and LAI observations has been investigated at a local scale. While in situ data are limited by their spatial coverage, EO satellite observations represent a significant source of information providing consistent data over large areas with a full spatial coverage. A wide range of satellite-based biophysical products have been developed within the FP7 Geoland2 project (http://www.gmes-geoland.info) as a key component of the Copernicus Global Land Service. It is an European initiative set up to operationally provide a set of biophysical

HESSD
10, 9057–9103, 2013

variables describing the terrestrial vegetation and the water and energy budgets. This work evaluates at the France scale the use of two satellite-based products provided by the Copernicus Global Land Service, namely SSM product retrieved from the scatterometer ASCAT together with GEOV1 LAI data in the vegetation growth version of the Interactions between Soil Biosphere Atmosphere model (ISBA-A-gs) (Calvet et al., 1998). The period under investigation extends over four years from 2008 to 2011 including various climatic conditions. In particular, the spring drought of 2011 is analyzed.

The main objectives of this study are to assess to what extent the LDAS is able to: (1) simultaneously ingest EO satellite data providing mixed signals at a grid-scale into the mosaic structure of ISBA-A-gs; (2) propagate information from the surface into the root-zone soil layer; (3) consistently impact the water and carbon fluxes; (4) improve the short-term vegetation response to drought conditions.

The ISBA-A-gs LSM, the observational data sets and the data assimilation scheme are described in Sect. 2. The LDAS configuration is presented in Sect. 3. In Sect. 4 the results are presented at the country scale, as well as over specific grid cells. The impact of the assimilation on LAI, soil moisture, water and carbon fluxes is presented in Sect. 4.3. Section 5.1 describes the impact of the assimilation on the monitoring of the drought of spring 2011. The verification of the assimilation impact on the root-zone soil moisture is performed using ground-based observations in Sect. 5.2. Finally, Sect. 6 summarizes the main conclusions of the study.

2 The LDAS

In this study, the LDAS is defined as an off-line sequential data assimilation system based on a LSM uncoupled with the atmosphere. The LDAS is able to integrate simultaneously available SSM and LAI observations at a given time step into the ISBA-A-gs LSM aiming at adjusting the model trajectory at that time. The experiments were conducted with the SURFEX modelling platform (Le Moigne et al., 2009) developed at Meteo-France, which represents the vegetation sub-grid heterogeneity (crops, grass-

HESSD
10, 9057–9103, 2013

lands, coniferous forests, broadleaf forests) by using a mosaic approach (Koster and Suarez, 1992). The model is driven by observation-based atmospheric forcing data which are derived from the SAFRAN (Système d'Analyse Fournissant des Renseignements Atmosphériques à la Neige) mesoscale analysis system at 8-km spatial resolution and hourly temporal sampling (Quintana-Segui et al., 2008). Atmospheric variables include precipitation, 2 m air temperature, 2 m specific humidity, wind speed, surface pressure, incoming solar radiation, and incoming long-wave radiation.

The three main components of the LDAS (land surface model, remote sensing data and analysis scheme) are detailed hereafter.

2.1 The ISBA-A-gs LSM

In the SURFEX platform (http://www.cnrm.meteo.fr/surfex/), the ISBA LSM (Noilhan and Mahfouf, 1996) describes the exchanges between soil, vegetation and atmosphere. In this study, version 7.2 of SURFEX is used.

The force-restore three-layer version of the soil model in ISBA is used in this study (Boone et al., 1999). The soil texture parameters (clay and sand proportions) are taken from the soil geographical database (BDGSF) of the French National Institute of Agronomic Research available at http://www.gissol.fr/programme/bdgsf/. For each model grid cell, the modelled soil moisture is partitioned into three variables: the simulated SSM (representative of the first soil centimetre), the volumetric root-zone soil moisture WG2 (defined for rooting depths depending on the vegetation type, with a maximum thickness of 2.5 m) and a volumetric soil moisture value WG3 in the recharge zone below the plant roots (with a maximum thickness of 1 m). Hereafter, the simulated SSM will be referred to as SSMmod. In the model, the propagation of surface information to root-zone layer relies on the force-restore dynamics of the model: SSMmod is forced by precipitation and evaporation and restored toward WG2.

The A-gs module of ISBA was developed to allow the simulation of photosynthesis and the growth of vegetation with different biomass reservoirs (Calvet et al., 1998). The linear relationship between the active biomass and LAI (defined as the green leaf area

HESSD
10, 9057–9103, 2013

per unit ground horizontal surface area) is expressed as:

$$B_a = \beta \cdot \mathrm{LAI}, \quad (1)$$

where β may depend upon vegetation type, nitrogen supply and climate. The vegetation biomass and LAI variables are governed by photosynthesis and evolve dynamically in response to weather and climate conditions. Namely, during the growing phase the net assimilation of CO_2 photosynthesis leads to plant growth from a minimum threshold set to either $1\,m^2\,m^{-2}$ for coniferous forest or $0.3\,m^2\,m^{-2}$ for other vegetation types. A deficit of photosynthesis sets off leaf biomass mortality that exceeds net assimilation. Consequently LAI drops down to its minimum value.

The photosynthetic activity depends on the vegetation types. The input soil and vegetation parameters are provided by the ECOCLIMAP-II global database (Faroux et al., 2013) which describes ecosystem classes and assigns them in twelve elementary land cover types (patches) at 1 km spatial resolution. Three of them represent patches without vegetation (bare soil, permanent snow and rocks). Over the France domain, the dominant ecosystems are grasslands (31 %), C3 croplands (24 %), deciduous forest (20 %), coniferous forests (11 %) and C4 croplands (4 %). Bare soil represents 8 % of the area. The mean root depths are of 1.5 m for herbaceous vegetation and 2 m for forests.

The water and energy budgets are calculated separately for each patch. ISBA-A-gs simulates the aggregation of carbon, water, and energy fluxes from the different patches. The modelled LAI at 8 km resolution is an average value of vegetation types (up to 9 in the current configuration) weighted with their cover fraction.

The ISBA A-gs model simulates the interaction between water and carbon cycles. The evapo-transpiration flux (ET) represents the sum of the evaporation of liquid water from the soil surface and from the vegetation, and the sublimation from the snow and soil ice. The net ecosystem CO_2 exchange (NEE) is given by the difference between the ecosystem respiration (RECO) and Gross Primary Production (GPP). The GPP represents the carbon uptake by photosynthesis. The RECO value departs from

HESSD
10, 9057–9103, 2013

a basal rate as a function of soil temperature and soil moisture (Albergel et al., 2010). Following Lafont et al. (2012) the respiration basal rate was calibrated by assuming an equilibrium between the ecosystem respiration and the vegetation carbon uptake over the whole 4 yr period of the simulations.

Also, the A-gs module features two different types of the plant response to drought, for both herbaceous vegetation (Calvet, 2000) and forests (Calvet et al., 2004). In the strategy called defensive or drought-avoiding, the plant increases the water use efficiency (WUE) in response to soil water stress, while in the offensive strategy or drought-tolerant, the WUE is stable or even decreases. While C3 crops and coniferous trees are associated to a drought-avoiding behaviour, C4 crops, grasslands and broadleaf trees are associated to a drought-tolerant behaviour (Calvet et al., 2012, 2004).

2.2 Remote sensing data sets

2.2.1 Satellite-derived SSM

The Advanced Scatterometer (ASCAT) is an active C-band microwave sensor on board the European METOP polar-orbiting satellite. The soil moisture information is derived from ASCAT radar backscatter coefficients delivered at 25 km resolution using a methodology developed at the Vienna University of Technology (TU-Wien). This method is based on a change detection approach originally developed for the active microwave instrument flown on-board the European satellites ERS-1 and ERS-2 (Wagner et al., 1999; Bartalis et al., 2007). An exponential filter in its recursive formulation (Albergel et al., 2008) is applied to this SSM product to estimate the soil water index (SWI) using a time scale parameter T that may vary between 1 day and 100 days. The result for the top soil moisture content (< 5 cm) range between 0 (dry) and 1 (saturated). Hereafter, this quantity will be referred to as SSMsat. In this study, SSMsat consists of Geoland2 soil water index values with a characteristic time length of one day, denoted by SWI-001 (Kidd et al., 2011).

HESSD
10, 9057–9103, 2013

A surface state flag which identifies either frozen conditions, presence of snow cover or temporary melting/water on the surface is provided. The product includes also a quality flag indicating the availability of SSMsat measurements with an acceptable quality.

After screening, the remaining data were projected onto the 8 km model grid resolution by assigning each observations to all SAFRAN grid cells within 0.15° and then considering the average of data assigned to each model grid. The model time series were compared with soil moisture data to determine their capability to represent the temporal dynamics at a grid scale. A good agreement between the SSMsat and the modelled SSM was found, despite anomalously low values of SSMsat produced in frozen surface conditions. These erroneous values are not adequately identified by the flags. This suggests that an additional frozen surface mask depending on model forecasts of frozen conditions has to be applied to the SSMsat data before being used in a data assimilation application. Similar to Draper et al. (2011), the screening procedure was extended to the use of two additional static masks in order to discard data in urban regions with a urban fraction greater than 15 %, and to remove data with a topographic flag representing mountainous regions with an altitude greater than 1500 m.

2.2.2 Satellite-derived LAI product

The GEOV1 LAI product developed within the Geoland2 project is derived from the SPOT-VGT satellite observations. Hereafter, this quantity will be referred to as LAIsat. The LAIsat values are produced by a statistical algorithm, namely a neural network trained using two pre-existing products: the SPOT-VGT CYCLOPES V3.1 product (Baret et al., 2007) and the TERRA/ AQUA MODIS collection 5 product (Myneni et al., 2002). The product is provided globally at a spatial resolution of 1 km and a 10 day sampling time in a Plate Carrée projection. The LAIsat is close to the true LAI since the saturation effect affecting the CYCLOPES product for large LAI values corresponding to dense canopies was reduced by the MODIS contribution in the training process.

HESSD
10, 9057–9103, 2013

The retrieval methodology and detailed information about the product are described by Baret et al. (2013).

Camacho et al. (2013) performed a validation study by comparing the GEOV1 product with ground measurements and other reference satellite products. They concluded that the GEOV1 is a reliable product and has an important added-value regarding its two precursor products.

A quality check was performed using a number of quality flags provided with the LAIsat. The data are kept only if all the quality flags are set to 0. The 1 km data are aggregated at the model grid at 8 km resolution if at least 32 grid points are present (more than half the maximum amount).

2.3 Data assimilation

In the simplified version of the EKF used in this study, namely SEKF, the background covariance matrix **B** does not evolve with time. The SEKF calculation of the analysis increment ($\Delta \boldsymbol{x}$) at time when an observation is available is given by:

$$\Delta \boldsymbol{x} = \mathbf{K}\left[\boldsymbol{y}^{\mathrm{o}} - H(\boldsymbol{x})\right], \tag{2}$$

where $\boldsymbol{x}$ is the state vector, and $\boldsymbol{y}^{\mathrm{o}}$ is the observation vector. **K** that represents the Kalman gain is calculated as in the following expression:

$$\mathbf{K} = \mathbf{B}\mathbf{H}^{\mathrm{T}}\left[\mathbf{H}\mathbf{B}\mathbf{H}^{\mathrm{T}} + \mathbf{R}\right]^{-1}. \tag{3}$$

Here **H** is the Jacobian matrix of the linearised observation operator H and $\mathbf{H}^{\mathrm{T}}$ represents its transpose. The covariance matrices of the background (**B**) and observation (**R**) errors are assumed diagonal.

As mentioned before, for the multi-patch version of the model, each model grid cell is split in a number of twelve patches each having their own prognostic variables. The filter algorithm is designed to provide the analysis for each patch independently by using one grid-wise observation. Therefore, the model counterpart of the observation

HESSD
10, 9057–9103, 2013

$\boldsymbol{y} = H(\boldsymbol{x})$ is assumed to be the average of the corresponding predicted observation for each patch $y_p = H(x_p)$ weighted with the fraction α_p occupied by each patch p:

$$\boldsymbol{y} = \sum \alpha_p H(x_p), \tag{4}$$

Since the patches are considered as independent and, then, the simulated observation over the patch only depends upon the state vector over the same patch, the elements of the Jacobian matrix $\mathbf{H}_p$ for each patch p are:

$$H_p{}^{mn} = \frac{\partial y^m}{\partial x_p^n} = \alpha_p \frac{\partial y_p^m}{\partial x_p^n}, \tag{5}$$

where the m and n indices hold for mth and nth components of observation and state vector, respectively. The elements of $\mathbf{H}_p$ are estimated using a finite difference approximation by perturbing individually each analyzed variable with a small perturbation $\delta x_p{}^n$:

$$\mathbf{H}_p{}^{mn} = \alpha_p \left[\frac{y_p{}^m(\boldsymbol{x} + \delta x_p{}^n) - y_p{}^m(x)}{\delta x_p{}^n} \right]. \tag{6}$$

Following a previous study (Barbu et al., 2011), the size of perturbations was set at $10^{-4} \times (w_{\mathrm{fc}} - w_{\mathrm{wilt}})$ for WG2 and at 10^{-3} for LAI as they were proved to lead to an acceptable linearisation of the Jacobian. w_{fc} and w_{wilt} represent the volumetric field capacity and the wilting point, respectively.

The Kalman gain is computed for each patch according to Eq. (3). A new value that represents the analysis for each patch p, denoted by $x_p{}^{\mathrm{a}}$ is obtained by adding the analysis increment obtained as in Eq. (2) to the background. Finally, the updated variable $\boldsymbol{x}^{\mathrm{a}}$ is aggregated from the weighted contribution of each patch over the grid as:

$$\boldsymbol{x}^{\mathrm{a}} = \sum \alpha_p x_p{}^{\mathrm{a}}. \tag{7}$$

HESSD
10, 9057–9103, 2013

Figure 1 illustrates an example of the multi-patch data assimilation scheme for a grid cell split into three patches. The aggregation and disaggregation arrows correspond to the calculation of the model counterparts of a grid-scale observation $\boldsymbol{y}^{o}$ and to the extraction of the data information distributed among the patches.

3 Description of the experimental design

A number of steps are necessary before assimilating the remote sensing data: projection of satellite data onto the 8 km model grid, bias correction using a Cumulative Distribution Function (CDF) matching technique applied to the ASCAT data and specifications of model and observation errors.

3.1 State vector and resolution

The root-zone soil moisture is of the great relevance to this study, as it governs the plant response to drought. Also, following a recommendation of Draper et al. (2009), the SSM variable was not analyzed and was excluded from the control vector in order to reduce the number of linearisation of the Jacobian. Indeed, due to the small size of its reservoir and its short memory, the SSM is less critical to analyse. Therefore, in this study, the control state vector for the analysis consists of two prognostic variables, root-zone soil moisture and LAI, each of them containing 12 values that correspond to the twelve patches. The vector of observations includes two elements: SSMsat and LAIsat at each grid cell.

The model simulations without data assimilation (prior) start in January 2007. The year 2007 is considered as a spin-up period for the model run in order to obtain an equilibrium state. Then, the assimilation experiment starts on 1 January 2008 and lasts until 31 December 2011. The SEKF assimilates available observations every 24 h at 09:00 UTC, by analysing the initial state via the information provided by an observation at the end of the assimilation window. The SSMsat observations are converted into

HESSD
10, 9057–9103, 2013

volumetric water content (see Sect. 3.2) and assumed to be the observation equivalent of the SSMmod. Possible mismatch between observed and modelled quantities are accounted for in a bias correction scheme described in the next section. Concerning LAI, the satellite-derived product is considered to be the observation equivalent of the simulated LAI. The LAIsat is assimilated at the provided temporal resolution of 10 days.

The LDAS products (LAI, root-zone soil moisture, water, carbon and energy fluxes) are provided across the France domain split into 8602 grid cells, each of them of 8 km resolution (Habets et al., 2008) at the temporal resolution of one day for the state variables LAI and soil moisture and as cumulated daily outputs for the fluxes. Hereafter, the analyzed variables will be referred to as posterior, in opposition to the modelled variables referred to as prior.

3.2 Rescaling and bias correction

Prior to assimilation, the SSMsat product has to be transformed into model equivalent volumetric SSM. The discrepancies between the model simulations and the satellite observations are addressed as part of the data assimilation system. The SSMsat data are rescaled by matching its CDF to that of SSMmod. The approach described in Scipal et al. (2008) permits correcting for the differences in the first two moments (mean and variance) of the distribution and can be viewed as a linear transformation. The two parameters of the linear relationship, the intercept a and the slope b vary spatially, but are constant in time:

$$a = \bar{\theta}_{\mathrm{m}} - b \times \bar{\theta}_{\mathrm{o}}, \tag{8}$$

$$b = \frac{\sigma_{\mathrm{m}}}{\sigma_{\mathrm{o}}}, \tag{9}$$

where $\bar{\theta}_{\mathrm{m}}$ and $\bar{\theta}_{\mathrm{o}}$ hold for the means of model and observation, respectively, while σ_{m} and σ_{o} represent the standard deviation errors for model and observations, respectively. Scipal et al. (2008) noted that the use of a linear transformation produces the

HESSD
10, 9057–9103, 2013

bias free observations (with respect to the model) for the entire considered period, but systematic differences related to seasonal or inter-annual variations in bias may remain uncorrected. The importance of accounting for seasonal corrections in the CDF matching was discussed for the AMSR-E (Advanced Microwave Scanning Radiometer) SSM data and the SSM provided by the NWP system ALADIN of Meteo-France by Draper et al. (2009).

Therefore, we have derived the *a* and *b* CDF matching parameters on a seasonal basis by using a three-month moving window from 2008 to 2011. The CDF matching moments are computed based on (1) screened observations with the quality flag provided with the SSMsat and additional aforementioned masks for altitude and urban fractions, and (2) SSMmod values for simulated soil temperature above 0 °C.

The model simulations were compared with the two CDF rescaled ASCAT time series to determine their capability for representing the temporal dynamics at two locations in North-East (48.199° N, 1.053° W) and in South-West (43.350° N, 1.302° E) of France (Fig. 2). For both locations, the CDF matching with seasonal correction improves the temporal correlations between the data and the model when compared with the approach without seasonal corrections from 0.72 to 0.79 (location in the North-East) and from 0.70 to 0.79 (location in the South-West). In addition, the seasonal bias correction reduces the standard deviation of the bias by 0.01 $m^3 m^{-3}$ for both locations.

One can notice low SSMsat values in May, especially in northern France as illustrated in Fig. 2 at local scale. Figure 3 shows that this characteristic is widespread in northern France. In the latter figure, the date of the annual minimum of SSMmod and of SSMsat as rescaled with the two CDF matching approaches are illustrated for the year 2009. The model simulates a minimum occurring in the summer period (after Day of Year (DOY) 200) across almost the full domain with few exceptions in the eastern part of France where the minimum is found around DOY 150 (left panel). The SSMsat minimum value is reached in May (before DOY150) over the northern and central regions (middle panel). This characteristic of ASCAT data is persistent over the entire

HESSD
10, 9057–9103, 2013

4 yr period. Using a seasonal CDF matching approach helps adjusting the date of the minimum SSMsat to that of SSMmod as is illustrated in the right panel of Fig. 3.

3.3 Background and observation errors

For simulated root-zone soil moisture, a mean volumetric standard deviation (std) error of 0.02 $m^3 m^{-3}$ was chosen as suggested by several authors (Mahfouf et al., 2009; Draper et al., 2011; Barbu et al., 2011). In this experiment, the observational error is set to 0.05 $m^3 m^{-3}$ according to the median value of SSMsat ASCAT data error estimates. This value is consistent with errors typically expected for remotely sensed soil moisture (de Jeu et al., 2008; Draper et al., 2011).

Similar to Mahfouf et al. (2010) and Dharssi et al. (2011), a background quality control is performed in order to reject SSMsat converted to volumetric soil moisture that are too far from the model first-guess. By assuming that the observation error is equal to SSMmod error, the data are discarded if the innovations (differences between observations and background) are larger than 0.21 $m^3 m^{-3}$ (i.e. three times the square root of the sum of the observation and background variances).

Concerning LAI, in a previous study, Barbu et al. (2011) estimated in situ LAI observation errors for grassland. Their results are difficult to extend to satellite-based LAI uncertainties at the France scale. In a recent study, Fang et al. (2013) estimated the average of the theoretical uncertainties of the GEOV1 product at the global scale. The theoretical uncertainties are related to the input data and retrieval processes and resemble random errors. They reported a std error value of 0.24 $m^2 m^{-2}$. In this study, the std errors of LAIsat is increased up to 0.3 in order to account for the additional uncertainties related to the aggregation procedure from 1 to 8 km resolution.

Generally, the start and the end of the growing season are considered being better represented by the satellite products (Jarlan et al., 2008; Brut et al., 2009; Szczypta et al., 2012). Preliminary tests showed that to ensure that the phenology derived from LAIsat is preserved, the observational errors have to be smaller than the model errors:

HESSD
10, 9057–9103, 2013

the std errors of LAImod is set to 0.6 $m^2 m^{-2}$. It has been checked that the observation and model error specifications are consistent with innovation statistics.

4 Results

4.1 Jacobian terms

The Jacobian of the observation operator (H) described in Sect. 2.3 is required to calculate the Kalman gain (Eq. 3). The histograms of Jacobian values corresponding to the $\frac{\partial \mathrm{LAI}(t)}{\partial \mathrm{LAI}(t_0)}$ Jacobian term for vegetated patches were computed (not shown). As already noted by Rüdiger et al. (2010), three types of Jacobian values can be identified for $\frac{\partial \mathrm{LAI}(t)}{\partial \mathrm{LAI}(t_0)}$ with ISBA-A-gs, each one corresponding to a distinct mode of the histograms: (1) identical to zero, (2) close to a maximal value equal to the fraction occupied by the plant functional type, and (3) a fraction of maximal value decreasing during the growing phase of the vegetation. This behaviour is common to all patches. The zero Jacobian value occurs when the LAI declines down to its minimal value in winter due to environmental conditions and also during drought periods. This non-informative Jacobian value has a larger frequency of occurrence in drought periods for the herbaceous vegetation types, as they are more sensitive than forests to the water stress.

Time series of daily Jacobian term $\frac{\partial \mathrm{LAI}(t)}{\partial \mathrm{WG2}(t_0)}$ for the year 2009 at one location (43.35° N, 1.30° E) in south-western France are illustrated in Fig. 4. The three main vegetated patches are present in the grid cell: C3 crops (48 %) depicted in blue, grassland (19 %) in green, and deciduous forest (9 %) in red. Bare soil represents 14 %. The black curve represents the normalized soil moisture NWG2 corresponding to the C3 crop patch. The NWG2 is defined as:

$$\mathrm{NWG2} = \frac{\mathrm{WG2} - w_{\mathrm{wilt}}}{w_{\mathrm{fc}} - w_{\mathrm{wilt}}}. \quad (10)$$

HESSD
10, 9057–9103, 2013

The dimensionless values of NWG2 are larger than 1 when the soil moisture content exceeds the volumetric field capacity and negative when the soil moisture content is below the wilting point meaning that the root water uptake stops. In a previous study, Barbu et al. (2011) analyzed the sensitivity of LAI to water perturbations in the rooting layer for grassland. They noted that, generally, the Jacobian term had positive values since an increase in water content directly impacted photosynthesis and plant growth. In this study, a noticeable feature concerns the existence of negative Jacobian values for the C3 crop patch. For normalized soil moisture values ranging between a given critical limit of 0.3 and 1, a moderate water stress is defined. In these conditions, a drought-avoiding strategy takes place. A decrease in soil moisture is characterized by an increase in the water use efficiency, which enhances photosynthesis. Therefore, between these limits, negative water perturbations can lead to an increase of the photosynthesis.

Large Jacobian values correspond to advanced stages of water stress. When the normalized soil moisture approaches zero, small increases in WG2 cause large increases in biomass production which reveals a specific non-linear behaviour of the ISBA-A-gs scheme. This behaviour is common to all patches. Null Jacobian values, indicating no sensitivity of LAI to soil moisture, occur when the water content is below the wilting point or above the volumetric field capacity.

4.2 Impact of assimilation on LAI and WG2 at patch level

Figure 5 shows for the year 2009 the prior and posterior LAI and WG2 daily evolutions per patch (top panels) and aggregated at pixel level (bottom panels) at the same location (43.35° N, 1.30° E) in south-western France. The root-zone soil moisture starts to decline in May and reaches a minimum in September (Fig. 5d), whereas LAI increases from March through May and remains high until July (Fig. 5c).

The LAI evolution between two assimilation steps for the two dominant vegetation types (crops and grassland) is rather similar. The LAI increments are distributed among the patches according to the fraction occupied by each patch in the model grid cell.

HESSD
10, 9057–9103, 2013

In spring, the positive increments are larger for C3 crops since they represent the main vegetation type within the grid cell. In summer, the temporal evolution of LAI per patch shows a more complex picture due to the combined effect of LAI and soil moisture analysis, and also, due to possible conflicting data information to be assimilated. Barbu et al. (2011) investigated the latter issue for grasslands. In a local experiment conducted over a semi-arid woodland Kato et al. (2013) also discusses the case of assimilating conflicting data streams (latent heat fluxes and FAPAR, in their case).

The impact of soil moisture changes on plant water availability is illustrated in Fig. 5a and b during the senescence phase. On one hand, the reduction in soil moisture content in June due to the assimilation contributes to a more rapid decrease of LAI. Then simultaneously assimilating the two data streams converges to a bias reduction in LAI. On the other hand, after this period, the slightly larger WG2 allows a vegetation regrowth both for cropland and grassland (a and b panels) not confirmed by observations. The assimilation of LAI draws back the model trajectory towards the lower observed LAI values by balancing between these two opposing tendencies in the data streams as it is clearly depicted in Fig. 5c at the grid scale.

The WG2 value shows a consistent seasonality among the patches, presenting a higher dynamic range for vegetated areas than for bare soil, in relation to the water uptake by the plants. At wintertime and early springtime, there are no significant differences between the vegetated patches and bare soil.

Finally, despite the spatial heterogeneity of a 8 km grid cell and the complex behaviour of each vegetation type at sub-pixel level, the assimilation is able to successfully exploit a mixed information and to come up with improved updated values aggregated at the grid scale.

4.3 Impact of assimilation on LAI, WG2 and fluxes at grid level

Before assimilation, LAIsat was compared to the model simulations over the France domain. Figure 6 presents the LAI time series for the model (referred to as prior), LAIsat data and assimilation (referred to as posterior) averages over France, respectively.

HESSD
10, 9057–9103, 2013

The annual cycles are rather different from one year to another. In 2008 the model has the longest cycle and the highest LAI maximum, while the satellite data show the largest LAI maximum in 2009. In 2011 LAI has a different seasonal cycle. Unusually high temperatures and low amount of precipitation characterized the 2011 spring in France. In relation to these conditions, both LAIprior and LAIsat maximums are lower. A vegetation regrowth occurs in August 2011 after rainfall events.

In a previous study, Lafont et al. (2012) noted systematic differences between the maximum LAI simulated by ISBA-A-gs and the LAI derived from two remote sensing products, namely CYCLOPES and MODIS over France, as well as in the timing of the phenological cycle. In this study, comparison between LAIprior and LAIsat reveals a good agreement in terms of amplitude and in terms of inter-annual variability. In contrast, the model simulations show a shifted phenology compared to the one observed by the satellite. Among causes that determine the mismatch between the model and the data, one can mention the differences in LAI values at the beginning of the growing cycle, LAIsat having larger values in winter (up to $1\,m^2\,m^{-2}$) than LAIprior (around $0.5\,m^2\,m^{-2}$). As a result, the start of the growing season tends to occur one month later in the model than in the observations. Similarly, the summertime senescence phase is delayed. The updated LAI shows a much better fit to the data over all the period. Indeed, the averaged correlation coefficient between LAIsat and the simulated LAI values increases from 0.58 for the prior LAI to 0.88 for the posterior LAI.

Figure 7 illustrates the maps of monthly averaged prior LAI, LAIsat and posterior LAI over France. At wintertime and in the early spring, the low LAI values already noticed reveal a bias between the model and the data. The spatial maps of satellite observations show higher LAI over many regions (Bretagne, Massif Central) from December to March. The assimilation is able to maintain higher LAI values over these regions, except in January. In March and April, the data assimilation increases the LAI values. As a consequence, the delay in the leaf onset is reduced. The start of declining LAIsat values occurs in July and is located over the agricultural areas in northern and southern France, as well as in the Mediterranean zone where the soil water stress is more

HESSD
10, 9057–9103, 2013

acute. In the model, the senescence occurs later following the same regional patterns as observed by satellite, but with a tendency to maintain high values until October. The lack of a detailed representation of the farming practices in the model (e.g. crop rotation and winter vs. summer crops) is then compensated by the assimilation. The simulated seasonal LAI cycle across crop regions is shifted towards the LAIsat cycle.

To evaluate the performance of the assimilation system, the innovations (differences between observations and background) and the residuals (differences between observations and analysis) were examined. Figure 8 illustrates the LAI monthly averages of innovations and residuals. One noticeable feature is the sign of the differences between LAIsat and LAIprior. In winter and spring, the simulated values are underestimated, while in rest of the period, corresponding to the senescence, they are overestimated. The assimilation tends to smooth out these differences, resulting in a less marked contrast between these two periods of the annual cycle with positive and negative increments of about the same magnitude. As expected, the residuals are smaller than innovations.

The changes operated in the seasonal LAI and WG2 cycles by the LDAS impact the seasonal and annual simulations of carbon and water fluxes. Figure 9 shows the average annual cycle over France of the relative differences (in units of %) between posterior and prior simulations with respect to prior simulations for LAI, WG2, evapotranspiration and GPP. The largest assimilation impact on LAI is obtained in early spring and ranges between +42.50 % and +89.8 %. Less marked LAI differences (between −20.6 % and −32.70 %) are noticed at the end of vegetation cycle. These relative differences in LAI are translated in terms of GPP relative differences with similar magnitude and seasonal behaviour. The impact of LAI updates on carbon fluxes is illustrated by the increased photosynthetic activity related to higher LAI values in the growing season (April) due to data assimilation corrections. In the same manner, the decrease in the CO_2 uptake during the senescence phase (August–September), when compared to the prior simulation, is related to lower LAI values. The changes in WG2 ranges between −3.33 % (May 2010) and 2.65 % (November 2011). The largest negative dif-

HESSD
10, 9057–9103, 2013

ferences occur in May for all years. Positive relative differences are obtained in the end of the summer and during autumn. The impact of the assimilation on evapotranspiration is less marked (the relative difference ranges between +20.4 % and −10.3 %). In March and April the acceleration of the vegetation growth by data assimilation tends to increase plant transpiration, for example up to 17.2 % in March 2011 and 20.4 % in April 2010. In the latter case, the augmentation of ET corresponds to an increased LAI of 61.3 %.

The LAI is an important driving variable for carbon and water fluxes, but the soil moisture has also a critical influence on the fluxes. Figure 10 shows the average monthly maps of LAI and WG2 increments and of the differences between the posterior and prior water fluxes (evapotranspiration and drainage). At wintertime, from December to February, the increments in WG2 present low values due to the reduced sensitivity of the Jacobian values during the widespread rainy episodes in this period. As the updated WG2 exceeds a maximum threshold (field capacity), the excess of water is drained out. In these conditions, small variations in WG2 may lead to large variations in total runoff. This impacts the drainage in winter within around 10 %. In the same period, the positive LAI increments help the model to adjust its minimum values to those of LAIsat. Due to the limited energy regime and the low vegetation activity the evapotranspiration is not sensitive to soil moisture and LAI changes.

In November, positive increments in WG2 are accumulated across the northern and central parts of France. The analysis increments are translated into drainage rather than in other components of the water budget as already noticed by Draper et al. (2011). This results in an important drainage flux in December. The process is amplified by the lower evapotranspiration rate due to lower incoming energy, as well as by the advanced phase of the senescence.

In March and April, positive increments in both LAI and WG2 lead to an augmentation of water fluxes. In contrast, negative soil moisture corrections are applied in May across the domain. This is due to the combined effects of the LAI and the soil moisture analysis. The assimilation of ASCAT data is the main contributor to the total correc-

HESSD
10, 9057–9103, 2013

tions (by 73 % on average) and tends to reduce WG2. In addition, the assimilation of LAI data into the model increases the vegetation biomass via increased LAI values and, consequently, the plant transpiration.

In June the assimilation starts to impact negatively on the LAI values, but shows a large increase in soil moisture content. As a consequence, the vegetation is less stressed and a positive rate of transpiration is maintained with few exceptions in Bretagne and in the Mediterranean region. In July and August the maps of evapotranspiration fluxes show more heterogeneous patterns. One can notice a tendency for reduced ET fluxes over the large agricultural area in northern France. In August, positive soil moisture increments across the western part of France are sufficient to maintain a higher rate of evapotranspiration.

Under dry conditions, evaporation is highly sensitive to soil moisture, but with limited values and variations (Seneviratne et al., 2010). This regime is relevant over the Mediterranean area in summer. The negative soil moisture increments show a decrease in soil moisture content that stresses vegetation, and evapotranspiration is thus reduced.

5 Discussion

5.1 Impact of assimilation on vegetation response to drought

Drought monitoring is a research field of major interest. The importance of the complex ecological and hydrological responses of ecosystems to drought has been highlighted in a number of studies (van der Molen et al., 2011; Hirschi et al., 2011; Ciais et al., 2005). Our interest is on the short-term responses of vegetation to agricultural drought, and to their impact on the deficit of soil moisture.

As mentioned before, the spring 2011 was characterised by the most severe drought recorded in the last 50 yr in France. According to Meteo-France (http://climat.meteofrance.com), spring rainfall deficits of more than half compared to long-term

HESSD
10, 9057–9103, 2013

mean were associated with temperatures up to 2.5 °C above normal, more than in 2007 (+2.1 °C) and in 2003 (+1.8 °C). The deficit of precipitation was generally more marked on the north-western two-thirds of the country. The average soil moisture level recorded in May was similar to what could normally be found in July or August. Drought conditions were reduced in July, where precipitation was 30 % above normal.

In contrast to the drought of 2003 that occurred in the beginning of the senescence phase of vegetation, the drought in spring 2011 had an important impact on the vegetation development in the peak of its growing phase with a diminution of crop productivity (Sepulcre et al., 2012). As a result, low maximum LAI values are simulated by the model, as well as observed by satellite. While the two sources of information agree on the maximum and mean values of LAI (Fig. 6), they disagree on the timing of the effects caused by the drought. The remote sensing observations show an earlier response to the occurrence of the drought.

Figure 11 shows the change rate of LAI calculated over 10 day-periods and highlights the changes in the strength and duration in the vegetation development. Unusually low LAIsat values are detected in April over the western part of France, while the model does not detect the negative changes before the end of May.

On one hand, the most severe decreases in LAIsat values are observed in the middle and the end of June over large regions, while in the first 20 day period in July the evolution of LAI is much steadier. On the other hand, the model shows similar pronounced negatives changes, but during the first 20 days of July, with a steadier evolution in the last 10 days of July.

In the LDAS configuration, the analysis is able to produce an earlier decline in LAI values. The temporal shift in the vegetation response to the severe water stress is about 20 days earlier in the western part of France and about 10 days earlier in the central parts of the domain. The negative trend in the LAI evolution extends to the first period of July, without reaching a steady state. In the end of July, the changes in the posterior LAI are close to the LAIsat with a clear positive trend in the south-western and central regions of France. The model response to the precipitation that occurs in

HESSD
10, 9057–9103, 2013

the second period of July is enhanced by the assimilation allowing a faster regrowth of the vegetation.

A significant reduction of modelled photosynthesis and CO_2 fluxes is experienced in June and July 2011. For example, in June, the mean reduction in GPP and NEE is of 31 and 45 % respectively, compared to the flux values averaged over the same month from 2008 to 2010. This period coincides also with a decline of evapotranspiration in response to a pronounced water deficit. Despite a temperature increase above average that tends to enhance the photosynthetic activity, the water stress has an adverse effect on GPP.

On the contrary, on an annual basis, the GPP and NEE fluxes at the France scale show a slight increase of 2.5 and 2 %, respectively, compared to the annual averages calculated for the period 2008–2010. This can be explained by an acceleration of the vegetation development at the beginning of the growing phase due to warmer-than-normal temperatures, as well as by an enlarged season of active biomass production after summer rainfalls. Actually, every month in 2011 was warmer-than-normal, with one noticeable exception in July. Then, the large reduction of the GPP fluxes in June and July is compensated by the positive impact of higher-than-average monthly temperatures in early spring and in autumn and a wetter-than-average summer. The LDAS does not change this tendency.

Figure 12 illustrates the change rate in the photosynthesis fluxes from one 10 day period to the next one. One can notice similar positive changes in the GPP fluxes in March and the first 10 days of April corresponding to the positive changes in LAI. In the last two-thirds of April, negative changes appear in the south-eastern regions and extend to the western and the central parts of France after assimilation, despite positive changes detected in LAI. From May to July the changes in GPP induced by analysis follow almost the same patterns as in the model, but with differences in intensity. For example, in the first two-thirds of May an increased reduction of photosynthetic activity in the western and in the central part of France is produced by the LDAS.

HESSD
10, 9057–9103, 2013

5.2 Verification using SMOSMANIA database

The scarcity of soil moisture and LAI in situ data limits the possibility of an independent validation of the assimilation results. In addition, point measurements are not necessarily representative of a coarser pixel scale, and thus, are difficult to interpret when compared to model results.

Despite the above limitation, the results of the assimilation were evaluated against the 12 SMOSMANIA (Soil Moisture Observing System-Meteorological Automatic Network Integrated Application) sites of Meteo-France located in the South West of France (Calvet et al., 2007). All of the stations are located in natural fallow.

The volumetric soil moisture values are derived from capacitance probes ThetaProbe ML2X of Delta-T Devices. Soil moisture observations are gathered at depths of 5, 10, 20, 30 cm, every 12 min. For this verification only measurements made at 30 cm were used.

Since the observations are representative only of the first 30 cm of soil, the impact of the analysis on WG2 is investigated by computing the absolute correlation and anomaly correlation between the simulated and observed soil moisture. The statistics are calculated at each station over the entire period. The measurements are compared to the simulated WG2 corresponding to the grassland patch. The anomaly time series are calculated by using a 30 day moving window as described in Draper et al. (2011). The significance level of correlations (p values < 0.01) was obtained for all stations. Soil moisture is in a good agreement with in situ measurements at the SMOSMANIA stations, with correlations higher than 0.7 which indicates that the model captures already well the soil moisture variability. Moreover, for two stations, the correlation coefficient is greater than 0.9. Generally, the correlations values do not vary significantly showing a low impact of the analysis. However, for all stations, the mean correlation is 0.82 without assimilation and 0.83 with assimilation. The anomaly correlations range between 0.3 and 0.7. The short-term variability is improved for eight stations. On average, the anomaly correlation increases from 0.57 to 0.58.

HESSD
10, 9057–9103, 2013

6 Conclusions

In the present study, a first attempt to use the multi-patch ISBA-A-gs land surface model in a multi-variate and multi-scale EO data assimilation experiment at a regional scale was made. The France domain encompasses a wide variety of soil and vegetation ecosystems. At 8 km pixel scale, there is a high degree of heterogeneity that should be taken into account. Each grid cell is represented as a mosaic of 12 land covers or patches. The ISBA-A-gs LSM provides a detailed computation of the surface fluxes of energy, water and carbon at the sub-grid (patch) level and allows aggregating the information from different ecosystem types. Following this approach, a land data assimilation system was designed to produce the updated variables for each land cover by using one grid-scale observation. It was demonstrated that useful information can be extracted from the data signal at the grid level and distributed among the patch structure of the model.

The assimilation was performed over the France domain for a period of 4 yr from 2008 to 2011 using an extended Kalman filter in order to incorporate the SSM product derived from ASCAT together with the GEOV1 LAI satellite product. An important motivation for combining two sources of information within a land surface model is the expectation that they will contribute in a more coherent manner to reduce model uncertainties. At the same time, the use of different types of data at different resolutions may generate new challenges in the construction of an appropriate observation operator. However, it has been shown in this study that, even using a rather simple CDF matching procedure, meaningful information can be captured from the data and integrated in the model.

The model performance prior to assimilation was discussed in comparison with observations. Differences between observed and simulated LAI values were noticed at the beginning of the growing phase of the vegetation. An underestimation of photosynthesis under cold conditions together with a slight underestimation of the incoming solar radiation in the SAFRAN analysis (Szczypta et al., 2011), could contribute to the

HESSD
10, 9057–9103, 2013

aforementioned differences. These discrepancies were identified as being partially responsible for a one-month delay in the LAI seasonal cycle. The assimilation is able to significantly reduce this delay and, consequently, to increase the correlation between the model and the data by more than 30 %.

Errors affecting model simulations may be related to the distribution of bare soil and vegetation and may depend on the vegetation type. For example, croplands present more heterogeneities than grasslands and many processes of anthropogenic nature are not described for crops in the model. In this study, model errors were set to a single value for all patches. However, even under this simple assumption, the assimilation compensates for the lack of description of managed ecosystems, by reducing the duration of the crop phenological cycle that tends to be too long in the model. The choice of model error may be refined by assigning different error statistics to different ecosystems and make use of observed LAI at a finer resolution.

The assimilation results depend also to a large extent upon the quality of the data to be assimilated. On one hand, the data used in this study show potential within the land data assimilation. On the other hand, the remotely sensed SSM data exhibit a number of non-realistic low values associated with large uncertainties over densely vegetated areas (Kidd et al., 2011). This may be detrimental to analysis by causing too large soil moisture depletion. Nevertheless, this effect has been minimized thanks to the seasonal bias removal performed before the assimilation.

Many studies indicate the presence of systematic biases between the observations and the model outputs for soil moisture (Walker et al., 2003; De Lanoy et al., 2007) and LAI (Jarlan et al., 2008; Lafont et al., 2012). These biases have multiple origins related to model inputs, model physics or data retrieval procedures. Correcting only for the existing bias in observations without properly accounting for model uncertainties leads to suboptimal data assimilation results. Moreover, as noted by Draper et al. (2011), the use of a simplified EKF limits the possibility of introducing more sophisticated description of forecast error terms and addressing model bias issue. An adaptive EKF has to be developed in order to include a bias-aware assimilation in the LDAS.

HESSD
10, 9057–9103, 2013

The impact of the assimilation upon carbon and water fluxes was also studied. It was shown that changes in LAI and soil moisture influence consistently the CO_2 and water balances. The changes on the GPP fluxes produce smaller differences in their seasonal cycle than for the LAI, but they follow the same tendency with increased values in early spring and decreased values in autumn. The impact of the assimilation on evapotranspiration produces changes between 10 and 20 %. A noticeable fact is the reduction of the ET fluxes over large agricultural areas. In November and December, the assimilation provides positive soil moisture increments in the root-zone reservoir that causes a supply of water to be drained out. The increased drainage fluxes by assimilation together with the fact that the surface scheme ISBA has an excessive drainage rate (Decharme et al., 2011) indicate that the assimilation leads to important river discharge changes. A comparison against in situ observations of soil moisture shows a positive impact of the assimilation on the root-zone soil moisture.

A lagged response of vegetation to the soil moisture deficit in the root zone was pointed out. A single, thick root-zone soil layer represents the soil hydrology in the model version used in this study. Such description increases the time to deplete soil moisture causing this slow response to dry conditions. Also, the propagation of surface soil moisture information within deeper layers may be affected by the lack of vertical resolution of the model. In that respect, a multi-layer version of the soil hydrology is expected to improve the overall performance of the system. Increasing the number of soil layers will allow an explicit representation of a vertical distribution of the root profile in the soil and then, a more realistic vegetation response to water stress. Moreover, the short-term effects of the severe drought of 2011 on the vegetation development were analysed. It was shown that the assimilation helped the model to better respond to the drought conditions and also to react more efficiently to rainfall events after the drought period. This may be particularly useful to analyse the impact of extreme climate conditions.

HESSD
10, 9057–9103, 2013

Acknowledgements. This work is a contribution to the Geoland2, IMAGINES and CORE-CLIMAX projects, co-funded by the European Commission within the Copernicus initiative in FP7. Constructive discussions with Clara Draper and Patricia de Rosnay are gratefully acknowledged.

The publication of this article is financed by CNRS-INSU.

References

Albergel, C., Rüdiger, C., Pellarin, T., Calvet, J.-C., Fritz, N., Froissard, F., Suquia, D., Petitpa, A., Piguet, B., and Martin, E.: From near-surface to root-zone soil moisture using an exponential filter: an assessment of the method based on in-situ observations and model simulations, Hydrol. Earth Syst. Sci., 12, 1323–1337, doi:10.5194/hess-12-1323-2008, 2008. 9064

Albergel, C., Calvet, J.-C., Gibelin, A.-L., Lafont, S., Roujean, J.-L., Berne, C., Traullé, O., and Fritz, N.: Observed and modelled ecosystem respiration and gross primary production of a grassland in southwestern France, Biogeosciences, 7, 1657–1668, doi:10.5194/bg-7-1657-2010, 2010. 9064

Barbu, A. L., Calvet, J.-C., Mahfouf, J.-F., Albergel, C., and Lafont, S.: Assimilation of Soil Wetness Index and Leaf Area Index into the ISBA-A-gs land surface model: grassland case study, Biogeosciences, 8, 1971–1986, doi:10.5194/bg-8-1971-2011, 2011. 9060, 9067, 9071, 9073, 9074

Baret, F., Hagolle, O., Geiger, B., Bicheron, P., Miras, B., Huc, M., Berthelot, B., Weiss, M., Samain, O., Roujean, J. L., and Leroy, M.: LAI, fAPAR and fCover CYCLOPES global products derived from VEGETATION. Part 1: Principles of the algorithm, Remote Sens. Environ., 110, 275–286, 2007. 9065

Baret, F., Weiss, M., Lacaze, R., Camacho, F., Makhmarad, H., Pacholczyk, P., and Smetse, B.: GEOV1: LAI, FAPAR essential climate variables and FCOVER global time series capitaliz-

HESSD

10, 9057–9103, 2013

ing over existing products. Part 1: Principles of development and production, Remote Sens. Environ., doi:10.1016/j.rse.2012.12.027, in press, 2013. 9066
Bartalis, Z., Wagner, W., Naeimi, V., Hasenauer, S., Scipal, K., Bonekamp, H., Figa, J., and Anderson, C.: Initial soil moisture retrievals from the METOP-A advanced Scatterometer (ASCAT), Geophys. Res. Lett., 34, L20401, doi:10.1029/2007GL031088, 2007. 9064
Bolten, J. D. and Crow, W. T.: Improved prediction of quasi-global vegetation conditions using remotely-sensed surface soil moisture, Geophys. Res. Lett., 39, L19406, doi:10.1029/2012GL053470, 2012. 9059
Boone, A., Calvet, J.-C., and Noilhan, J.: Inclusion of a third soi layer in a land surface scheme using the force-restore method, J. Appl. Meteor., 38, 1611–1630, 1999. 9062
Brut, A., Rüdiger, C., Lafont, S., Roujean, J.-L., Calvet, J.-C., Jarlan, L., Gibelin, A.-L., Albergel, C., Le Moigne, P., Soussana, J.-F., Klumpp, K., Guyon, D., Wigneron, J.-P., and Ceschia, E.: Modelling LAI at a regional scale with ISBA-A-gs: comparison with satellite-derived LAI over southwestern France, Biogeosciences, 6, 1389–1404, doi:10.5194/bg-6-1389-2009, 2009. 9071
Calvet, J.-C.: Investigating soil and atmospheric plant water stress using physiological and micrometeorological data sets, Agr. Forest Meteorol., 103, 229–247, 2000. 9064
Calvet, J.-C., Noilhan, J., Roujean, J.-L., Bessemoulin, P., Cabelguenne, M., Olioso, A., and Wigneron, J.-P.: An interactive vegetation SVAT model tested against data from six contrasting sites, Agr. Forest Meteorol., 92, 73–95, 1998. 9061, 9062
Calvet, J.-C., Rivalland, V., Picon-Cochard, C., and Guelh, J.-M.: Modelling forest transpiration and CO_2 fluxes-response to soil moisture stress, Agr. Forest Meteorol., 124, 143–156, doi:10.1016/j.agrformet.2004.01.007, 2004. 9064
Calvet, J.-C., Fritz, N., Froissard, F., Sequia, D., Petitpa, A., and Piguet, B.: In situ soil moisture observations for the CAL/VAL of SMOS: the SMOSMANIA network, International Geoscience and Remote Sensing Symposium, IGARSS, Barcelona, Spain, 23–28 July 2007, 1196–1199, doi:10.1109/IGARSS.2007.4423019, 2007. 9081
Calvet, J.-C., Lafont, S., Cloppet, E., Souverain, F., Badeau, V., and Le Bas, C.: Use of agricultural statistics to verify the interannual variability in land surface models: a case study over France with ISBA-A-gs, Geosci. Model Dev., 5, 37–54, doi:10.5194/gmd-5-37-2012, 2012. 9064
Camacho, F., Cernicharo, J., Lacaze, R., Baret, F., and Weiss, M.: GEOV1: LAI, FAPAR essential climate variables and FCOVER global time series capitalizing over existing prod-

HESSD
10, 9057–9103, 2013

ucts. Part 2: Validation and intercomparison with reference product, Remote Sens. Environ., doi:10.1016/j.rse.2013.02.030, in press, 2013. 9066

Ciais, P., Reichstein, M., Viovy, N., Granier, A., Ogée, J., Allard, V., Aubinet, M., Buchmann, N., Bernhofer, C., Carrara, A., Chevallier, F., De Noblet, N., Friend, A. D., Friedlingstein, P., Grünwald, T., Heinesch, B., Keronen, P., Knohl, A., Krinner, G., Loustau, D., Manca, G., Matteucci, G., Miglietta, F., Ourcival, J. M., Papale, D., Pilegaard, K., Rambal, S., Seufert, G., Soussana, J. F., Sanz, M. J., Schulze, E. D., Vesala T., and Valentini, R.: Europe-wide reduction in primary productivity caused by the heat and drought in 2003, Nature, 437, 529–533, doi:10.1038/nature03972, 2005. 9078

Crow, W. T. and van den Berg, M. J.: An improved approach for estimating observation and model error parameters for soil moisture data assimilation, Water Resour. Res., 46, W12519, doi:10.1029/2010WR009402, 2010.

De Lannoy, G. J. M., Reichle, R. H., Houser, P. R., Pauwels, V. R. N., and Verhoest, N. E. C.: Correcting for forecast bias in soil moisture assimilation with the ensemble Kalman filter, Water Resour. Res., 43, W09410, doi:10.1029/2006WR005449, 2007. 9083

De Rosnay, P., Drusch, M.,Vasiljevic, D., Balsamo, G., Albergel, C., and Isaksen, L.: A simplified Extended Kalman Filter for the global operational soil moisture analysis at ECMWF, Q. J. Roy. Meteorol. Soc., doi:10.1002/qj.2023, 2012. 9059

de Jeu, R. A. M., Wagner, W., Holmes, T. R. H., Dolman, A. J., van de Giesen, N. C., and Friesen, J.: Global soil moisture patterns observed by space borne microwave radiometers and scatterometers, Surv. Geophys., 29, 399–420, 2008. 9071

Decharme, B., Boone, A., Delire, C., and Noilhan, J.: Local evaluation of the Interaction between Soil Biosphere Atmosphere soil multilayer diffusion scheme using four pedotransfer functions, J. Geophys. Res., 116, D20126, doi:10.1029/2011JD016002, 2011. 9084

Demarty, J., Chevallier, F., Friend, A. D., Viovy, N., Piao, S., and Cias, P.: Assimilation of global MODIS leaf area index retrievals within a terrestrial biosphere model, Geophys. Res. Lett., 34, L15402, doi:10.1029/2007GL030014, 2007. 9059

Dharssi, I., Bovis, K. J., Macpherson, B., and Jones, C. P.: Operational assimilation of ASCAT surface soil wetness at the Met Office, Hydrol. Earth Syst. Sci., 15, 2729–2746, doi:10.5194/hess-15-2729-2011, 2011. 9059, 9071

Draper, C. S., Mahfouf, J.-F., and Walker, W.: An EKF assimilation of AMSR-E soil moisture into the ISBA land surface scheme, J. Geophys. Res., 114, D20104, doi:10.1029/2008JDO/1650, 2009. 9060, 9068, 9070

HESSD

10, 9057–9103, 2013

Draper, C., Mahfouf, J.-F., Calvet, J.-C., Martin, E., and Wagner, W.: Assimilation of ASCAT near-surface soil moisture into the SIM hydrological model over France, Hydrol. Earth Syst. Sci., 15, 3829–3841, doi:10.5194/hess-15-3829-2011, 2011. 9059, 9065, 9071, 9077, 9081, 9083

Fang, H., Jiang, C., Li, W., Wei, S., Baret, F., Chen, J. M., Garcia-Haro, J., Liang, S., Liu, R., and Myneni, R., Pinty, B., Xiao, Z., and Zhu, Z.: Characterization and intercomparison of global moderate resolution leaf area index (LAI) products: Analysis of climatologies and theoretical uncertainties, J. Geophys. Res.-Biogeo., 118, 1–20, doi:10.1002/jgrg.20051, 2013. 9071

Faroux, S., Kaptué Tchuenté, A. T., Roujean, J.-L., Masson, V., Martin, E., and Le Moigne, P.: ECOCLIMAP-II/Europe: a twofold database of ecosystems and surface parameters at 1 km resolution based on satellite information for use in land surface, meteorological and climate models, Geosci. Model Dev., 6, 563–582, doi:10.5194/gmd-6-563-2013, 2013. 9063

Garrigues, S., Lacaze, R., Baret, F., Morisette, J. T., Weiss, M., Nickeson, J. E., Fernandes, R., Plummer, S., Shabanov, N. V., Myneni, R. B., Knyazikhin, Y., and Yang, W.: Validation and intercomparison of global Leaf Area Index products derived from remote sensing data, J. Geophys. Res., 113, G02028, doi:10.1029/2007JG000635, 2008.

Gibelin, A.-L., Calvet, J.-C., Roujean, J.-L., Jarlan, L., and Los, S. O.: Ability of the land surface model ISBA-A-gs to simulate leaf area index at global scale: comparison with satellite products, J. Geophys. Res., 111, D18102, doi:10.1029/2005JD006691, 2006.

Gu, Y., Belair, S., Mahfouf, J. F., and Deblonde, G.: Optimal interpolation analysis of leaf area index using MODIS data, Remote Sens. Environ., 104, 283–296, doi:10.1016/j.rse.2006.04.021, 2006. 9059

Habets, F., Boone, A., Champeaux, J.-L., Etchevers, P., Franchist éguy, L., Leblois, E., Ledoux, E., Le Moigne, P., Martin, E., Morel, S., Noilhan, J., and Quintana-Seguì, P.: The SAFRAN-ISBA-MODCOU hydrometeorological model applied over France, J. Geophys. Res., 113, D06113, doi:10.1029/2007JD008548, 2008. 9069

Hirschi, M., Seneviratne, S. I., Alexandrov, V., Boberg, F., Boroneant, C., Christensen, O. B., Formayer, H., Orlowsky, B., and Stepanek, P.: Observational evidence for soil-moisture impact on hot extremes in southeastern Europe, Nat. Geosci., 4, 17–21, doi:10.1038/ngeo1032, 2011. 9078

Houser, P. R., Shuttleworth, W. J., Famiglietti, J. S., Gupta, H. V., Syed, K. H., and Goodrich, D. C.: Integration of soil moisture remote sensing and hydrologic modelling using

HESSD
10, 9057–9103, 2013

data assimilation, Water Resour. Res., 34, 3405–3420, doi:10.1029/1998WR900001, 1998. 9059

Jarlan, L., Balsamo, G., Lafont, S., Beljaars, A., Calvet, J.-C., and Mougin, E.: Analysis of leaf area index in the ECMWF land surface model and impact on latent heat on carbon fluxes: application to West Africa, J. Geophys. Res., 113, D24117, doi:10.1029/2007JD009370, 2008. 9059, 9060, 9071, 9083

Kaminski, T., Knorr, W., Scholze, M., Gobron, N., Pinty, B., Giering, R., and Mathieu, P.-P.: Consistent assimilation of MERIS FAPAR and atmospheric CO_2 into a terrestrial vegetation model and interactive mission benefit analysis, Biogeosciences, 9, 3173–3184, doi:10.5194/bg-9-3173-2012, 2012. 9060

Kato, T., Knorr, W., Scholze, M., Veenendaal, E., Kaminski, T., Kattge, J., and Gobron, N.: Simultaneous assimilation of satellite and eddy covariance data for improving terrestrial water and carbon simulations at a semi-arid woodland site in Botswana, Biogeosciences, 10, 789–802, doi:10.5194/bg-10-789-2013, 2013. 9060, 9074

Kidd, R., Makhmara, H., and Paulik, C. : BioPar Product User Manual Soil Water Index (SWI) – Version 2.0, GEOLAND2, 23 pp., available at: http://web.vgt.vito.be/documents/BioPar/g2-BP-RP-BP053-ProductUserManual-SWI-V2-I2.01.pdf, 2012. 9064, 9083

Koster, R. D. and Suarez, M. J.: Modeling the land surface boundary in climate modls as a composite of independent vegetation stands, J. Geophys. Res., 97, 2697–2715, 1992. 9062

Lafont, S., Zhao, Y., Calvet, J.-C., Peylin, P., Ciais, P., Maignan, F., and Weiss, M.: Modelling LAI, surface water and carbon fluxes at high-resolution over France: comparison of ISBA-A-gs and ORCHIDEE, Biogeosciences, 9, 439–456, doi:10.5194/bg-9-439-2012, 2012. 9064, 9075, 9083

Le Moigne, P., Boone, A., Calvet, J.-C., Decharme, B., Faroux, S., Gibelin, A.-L., Lebeaupin, C., Mahfouf, J.-F., Martin, E., Masson, V., Mironov, D., Noilhan, J., Tulet, P., and Van Den Hurk, B.: SURFEX scientific documentation, Groupe de météorologie à moyenne échelle, note de centre, 87, 211 pp., Meteo-France, Toulouse, 2009. 9061

Mahfouf, J.-F.: Assimilation of satellite-derived soil moisture from ASCAT in a limited-area NWP model, Q. J. Roy. Meteor. Soc., 136, 784–798, doi:10.1002/qj.602, 2010. 9059, 9071

Mahfouf, J.-F., Bergaoui, K., Draper, C., Bouyssel, F., Taillefer, F., and Taseva, L.: A comparison of two off-line soil analysis schemes for assimilation of screen level observations, J. Geophys. Res., 114, D08105, doi:10.1029/2008JD011077, 2009. 9060, 9071

HESSD
10, 9057–9103, 2013

Montzka, C., Pauwels, R. N. V., Franssen, H-j. H., Han, X., and Vereecken, H.: Multivariate and multiscale data assimilation in terrestrial systems: a review, Sensors, 12, 16291–16333, 2012. 9060

Myneni, R. B., Hoffman, S., Knyazikhin, Y., Privette, J. L., Glassy, J., Tian, Y., Wang, Y., Song, X., Zhang, Y., Smith, G. R., Lotsch, A., Friedl, M., Morisette, J. T., Votava, P., Nemani, R. R., and Running, S. W.: Global products of vegetation leaf area and fraction of absorbed PAR from one year of MODIS data, Remote Sens. Environ., 83, 214–231, 2002. 9065

Nearing, G. S., Crow, W. T., Thorp, K. R., Moran, M. S., Reichle, R., and Gupta, H. V.: Assimilating remote sensing observations of leaf area index and soil moisture for wheat yield estimates: An observing system simulation experiment, Water Resour. Res. 48, W05525, doi:10.1029/2011WR011420, 2012. 9060

Noilhan J. and Mahfouf, J.-F.: The ISBA land surface parameterisation scheme, Global Planet. Change, 13, 145–149, 1996. 9062

Pauwels, V. R. N., Verhoest, N. E. C., De Lannoy, G. J. M., Guissard V., Lucau C, and Defourny, P.: Optimization of a coupled hydrology–crop growth model through the assimilation of observed soil moisture and leaf area index values using an ensemble Kalman filter, Water Resour. Res., 43, W04421, doi:10.1029/2006WR004942, 2007. 9060

Quintana-Segui, P., Lemoigne, P., Durand, Y., Martin, E., Habets, F., Baillon, M., Canellas, C., Franchist éguy, L., and Morel, S.: Analysis of near surface atmospheric variables: Validation of the SAFRAN analysis over France, J. Appl. Meteorol. Clim., 47, 92–107, 2008. 9062

Reichle, R. H. and Koster, D.: Bias reduction in short records of satellite soil moisture, Geophys. Res. Lett., 31, L19501, doi:10.1029/2004GL020938, 2004.

Reichle, R. H., McLaughlin, D. B., and Entekhabi, D.: Hydrologic data assimilation with the ensemble Kalman filte, Mon. Weather Rev., 130, 103–144, 2002. 9059

Reichstein, M., Papale, D., Valentini, R., Aubinet, M., Bernhofer, C., Knohl, A., Laurila, T., Lindroth, A., Moors, E., Pilegaard, K., and Seufer, G.: Determinants of terrestrial ecosystem carbon balance inferred from European eddy covariance flux sites, Geophys. Res. Lett., 34, L01402, doi:10.1029/2006GL027880, 2007. 9059

Rüdiger, C., Albergel, C., Mahfouf, J.-F., Calvet, J.-C., and Walker, J. P.: Evaluation of Jacobians for Leaf Area Index data assimilation with an extended Kalman filter, J. Geophys. Res., 115, D09111, doi:10.1029/2009JD012912, 2010. 9072

HESSD
10, 9057–9103, 2013

Sabater, J. M., Rüdiger, C., Calvet, J.-C., Fritz, N., Jarlan, L., and Kerr, Y.: Joint assimilation of surface soil moisture and LAI observations into land surface model, Agr. Forest Meteorol., 148, 1362–1373, doi:10.1016/j.agrformet.2008.04.003, 2008. 9060

Scipal, K., Drusch, M., and Wagner, W.: Assimilation of a ERS scatterometer derived soil moisture index in the ECMWF numerical weather prediction system, Adv. Water Resour., 31, 1101–1112, doi:10.1016/j.advwatres.2008.04.013, 2008. 9069

Seneviratne, S. I., Corti, T., Davin, E. L., Hirschi, M., Jaeger, E. B., Lehner, I., Orlowsky, B., and Teuling, A. J.: Investigating soil moisture-climate interactions in a changing climate: a review, Earth-Sci. Rev., 99, 125–161, doi:10.1016/j.earscirev.2010.02.004., 2010. 9078

Sepulcre-Canto, G., Horion, S., Singleton, A., Carrao, H., and Vogt, J.: Development of a Combined Drought Indicator to detect agricultural drought in Europe, Nat. Hazards Earth Syst. Sci., 12, 3519–3531, doi:10.5194/nhess-12-3519-2012, 2012. 9079

Szczypta, C., Calvet, J.-C., Albergel, C., Balsamo, G., Boussetta, S., Carrer, D., Lafont, S., and Meurey, C.: Verification of the new ECMWF ERA-Interim reanalysis over France, Hydrol. Earth Syst. Sci., 15, 647–666, doi:10.5194/hess-15-647-2011, 2011. 9082

Szczypta, C., Decharme, B., Carrer, D., Calvet, J.-C., Lafont, S., Somot, S., Faroux, S., and Martin, E.: Impact of precipitation and land biophysical variables on the simulated discharge of European and Mediterranean rivers, Hydrol. Earth Syst. Sci., 16, 3351–3370, doi:10.5194/hess-16-3351-2012, 2012. 9071

van der Molen, M. K., Dolman A. J., Ciais, P., Eglin, T., Gobron, N., Law, B. E. , Meir, P., Peters, W., Phillips, O. L., Reichstein, M., Chen, T., Dekker, S. C., Doubková, M., Friedl, M. A., Jung, M., van den Hurk, B. J. J. M. , de Jeu, R. A. M., Kruijt, B., Ohta, T., Rebel, K. T., Plummer, S., Seneviratne, S. I., Sitch, S., Teuling, A. J., van der Werf, G. R., and Wang, G.: Drought and ecosystem carbon cycling, Agr. Forest Meteorol., 151, 765–773, doi:10.1016/j.agrformet.2011.01.018, 2011. 9059, 9078

Wagner, W., Lemoine, G., and Rott, H.: A method for estimating soil moisture from ERS scatterometer and soil data, Remote Sens. Environ., 70, 191–207, 1999. 9064

Walker, J. P., Houser, P. R., and Reichle, R.: New technologies require advances in hydrologic data assimilation, EOS T. Am. Geophys. Un., 84, 545–551, 2003. 9083

HESSD
10, 9057–9103, 2013

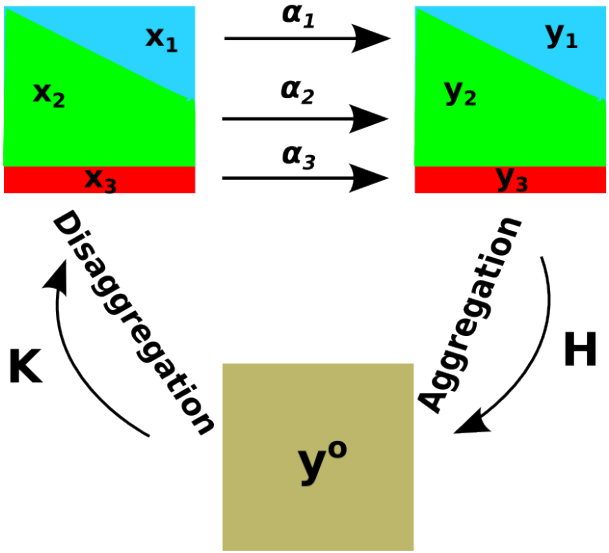

Fig. 1. The multi-patch data assimilation design for a grid cell split into three patches p each having their variables x_p. The predicted observations y_p are weighted with their fraction denoted by α_p, where $p \in 1,2,3$. $\boldsymbol{y}^o$ represents the grid-scale observation. The observation operator **H** aggregates the predicted observations at the grid scale (Eq. 4). The data information is split among patches via the Kalman gain **K** (Eq. 2).

HESSD
10, 9057–9103, 2013

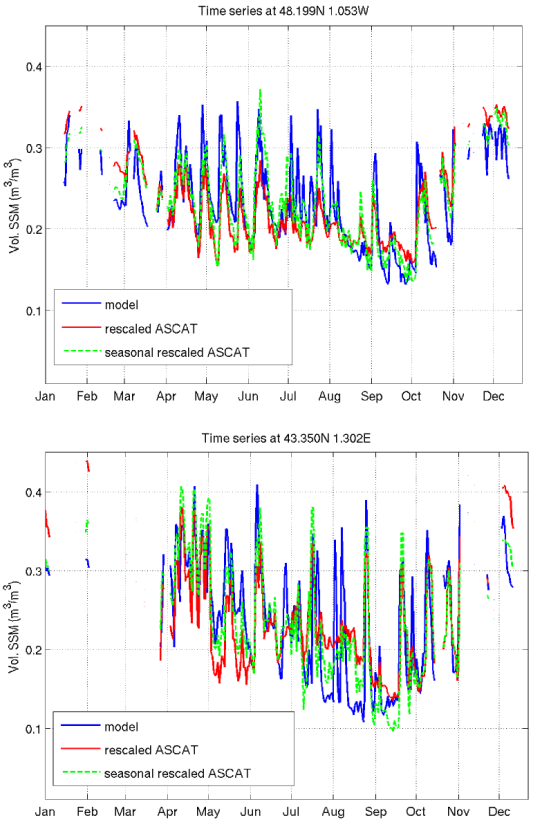

Fig. 2. Surface soil moisture evolutions for 2009 at two location in North East (top) and in South West (bottom) of France for model (blue), ASCAT CDF rescaled (red) and ASCAT seasonal CDF rescaled (green) observations.

HESSD
10, 9057–9103, 2013

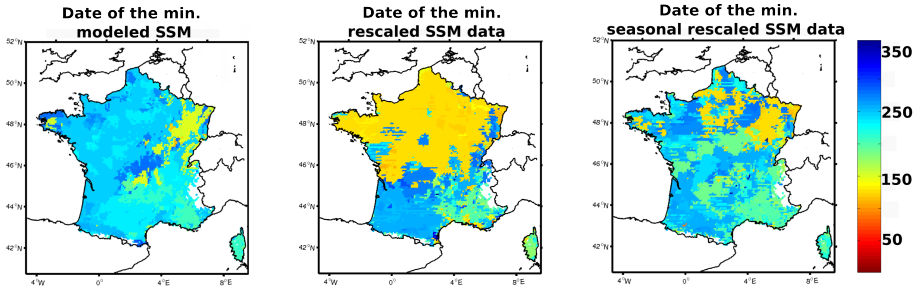

Fig. 3. Date of the lowest SSMmod values (left), CDF rescaled SSMsat (middle) and seasonal CDF rescaled SSMsat (right) for the year 2009 across the France domain. The colorbar represents the days of the year.

HESSD
10, 9057–9103, 2013

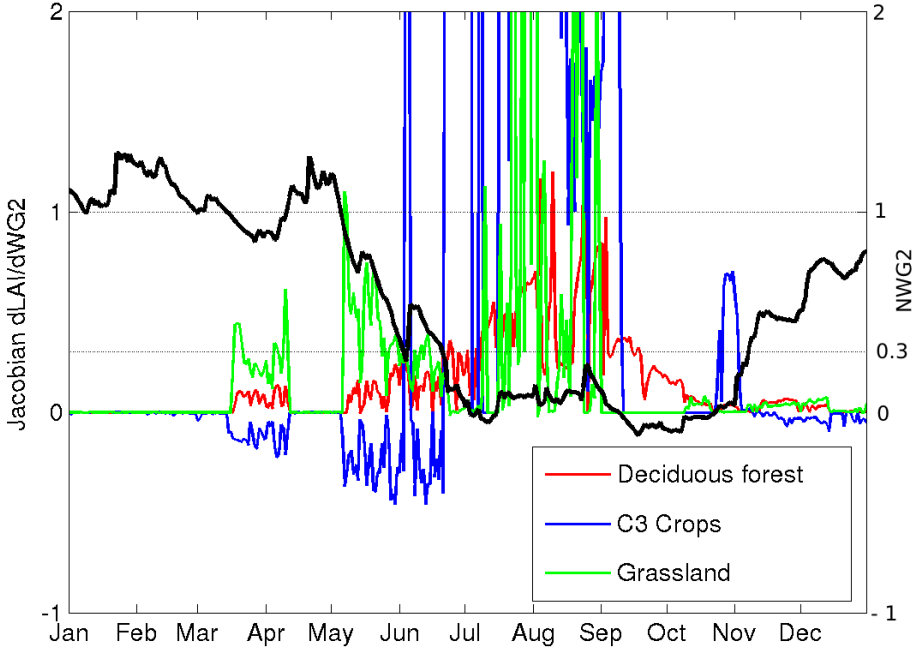

Fig. 4. Time series of daily Jacobian values for the majority patches (deciduous forest, C3 crops and grassland) at a location (43.35° N, 1.30° E) in South West of France for 2009. The simulated normalized soil moisture (NWG2) for the C3 crop patch is represented in black.

HESSD
10, 9057–9103, 2013

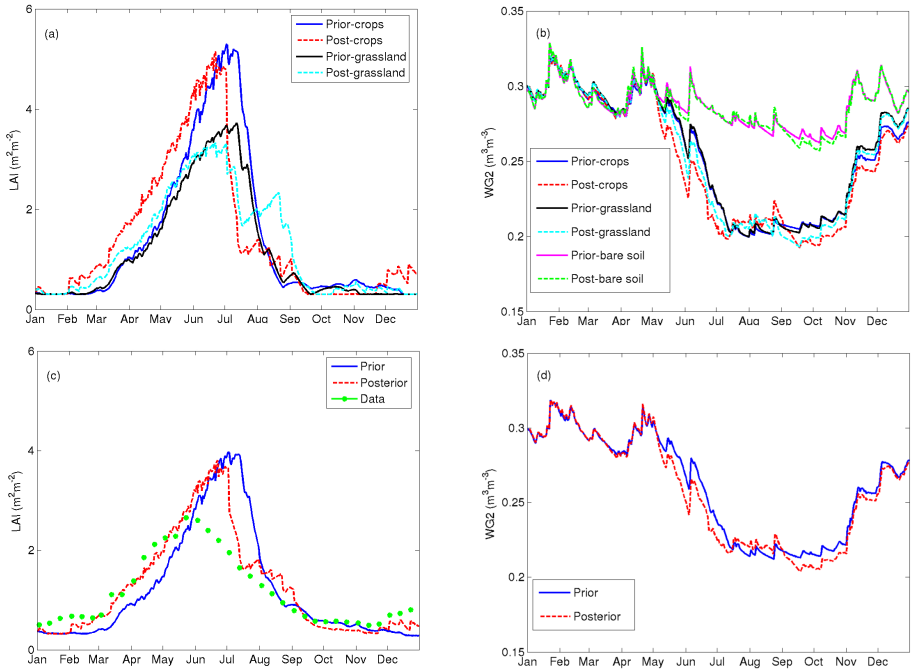

Fig. 5. Time series of prior and posterior LAI in $m^2\,m^{-2}$ (left) and volumetric root-zone soil moisture (right) per patches (top panels) and per grid cell (bottom panels) at a location (43.35° N, 1.30° E) for the year 2009. The majority patches are cropland (48 %), grassland (19 %) and bare soil (14 %). The LAI satellite data gathered at this location are depicted by stars.

HESSD
10, 9057–9103, 2013

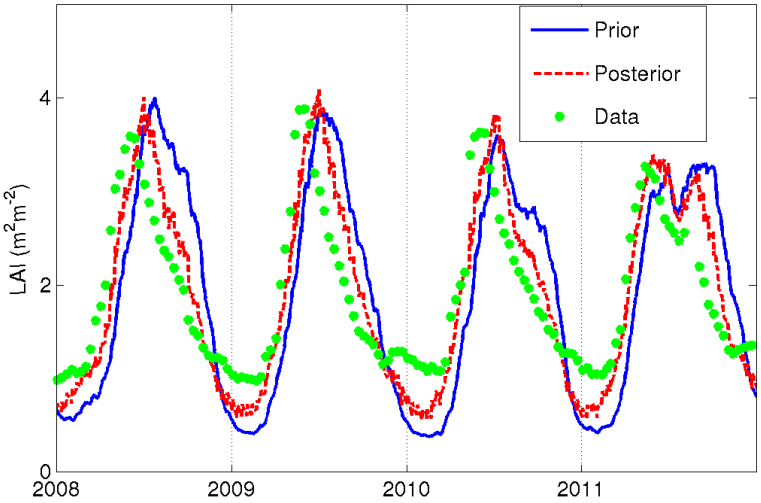

Fig. 6. Time series of prior (blue), observed (green) and posterior (red) LAI ($m^2\,m^{-2}$) averaged over France from 2008 to 2011.

HESSD
10, 9057–9103, 2013

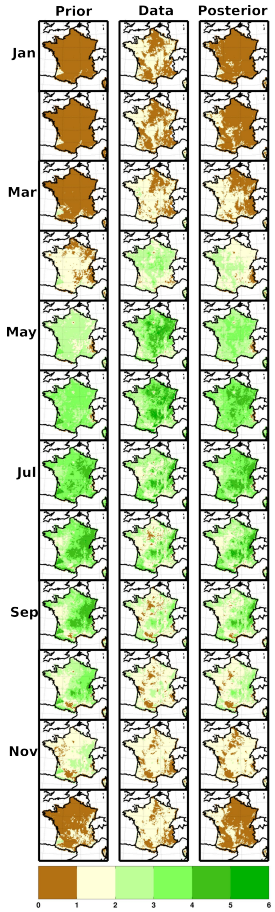

Fig. 7. Maps of monthly averages for prior (left), data (middle) and posterior (right) LAI over the period 2008–2011. The units are in $m^2\,m^{-2}$.

HESSD
10, 9057–9103, 2013

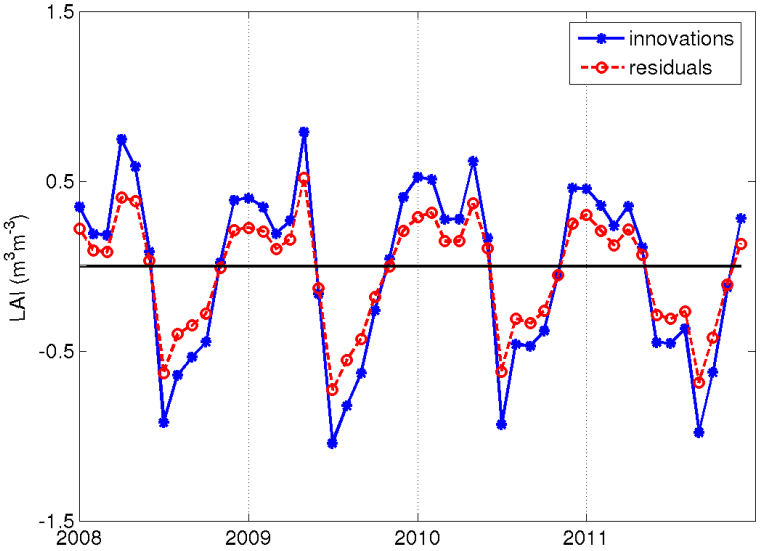

Fig. 8. Monthly evolution of LAI innovations (in blue) and residuals (in red) in $m^2 m^{-2}$ units averaged over France.

HESSD
10, 9057–9103, 2013

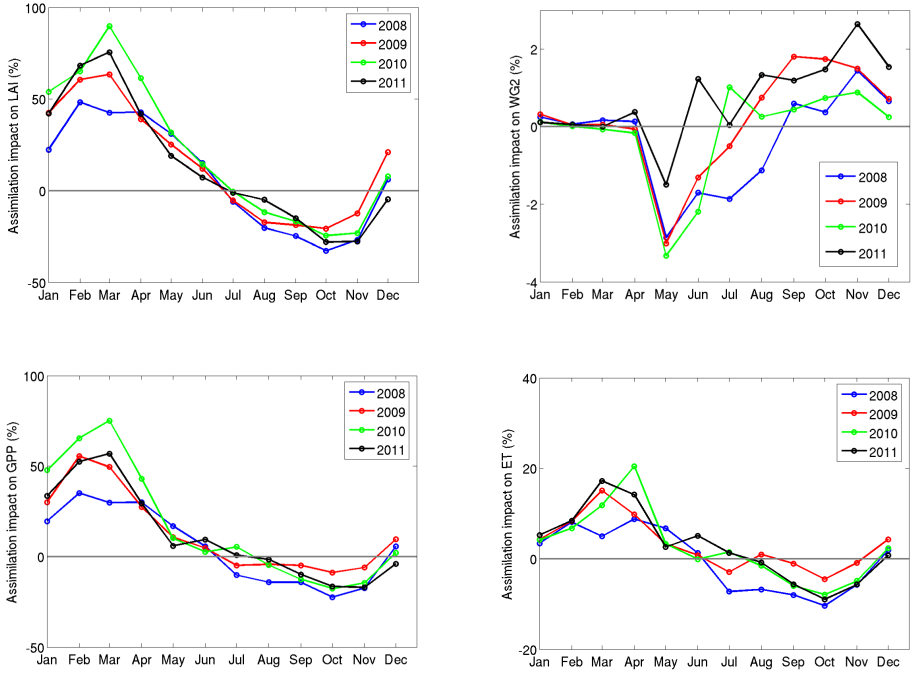

Fig. 9. Assimilation impact in terms of monthly relative differences (in percent) between the posterior and the prior spatial averages for LAI (top, left), soil moisture WG2 (top, right), GPP (bottom, left) and ET (bottom, right) fluxes, respectively.

HESSD
10, 9057–9103, 2013

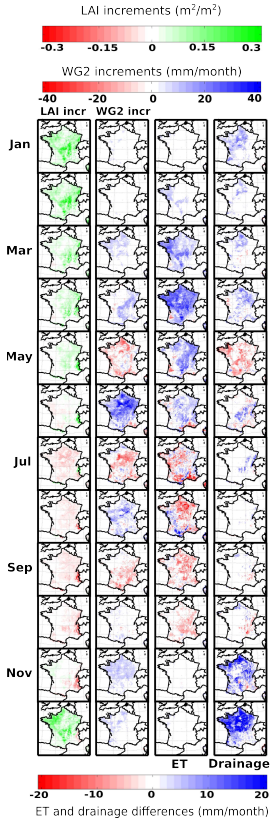

Fig. 10. Monthly maps of LAI (first column), soil moisture (second column) increments and the differences (posterior minus prior) for ET and drainage fluxes (third and fourth columns, respectively) averaged over 2008–2011. The units are in $m^2\,m^{-2}$ for LAI and in mm per month for water fluxes.

HESSD
10, 9057–9103, 2013

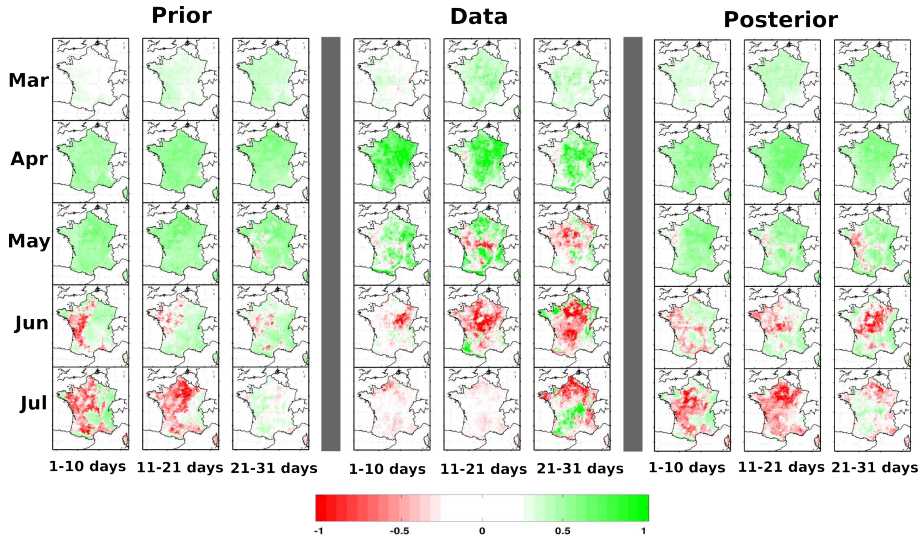

Fig. 11. Change rate calculated over 10 day period for prior, observed and posterior LAI from March to July 2011. The units are in $m^2\,m^{-2}$.

HESSD
10, 9057–9103, 2013

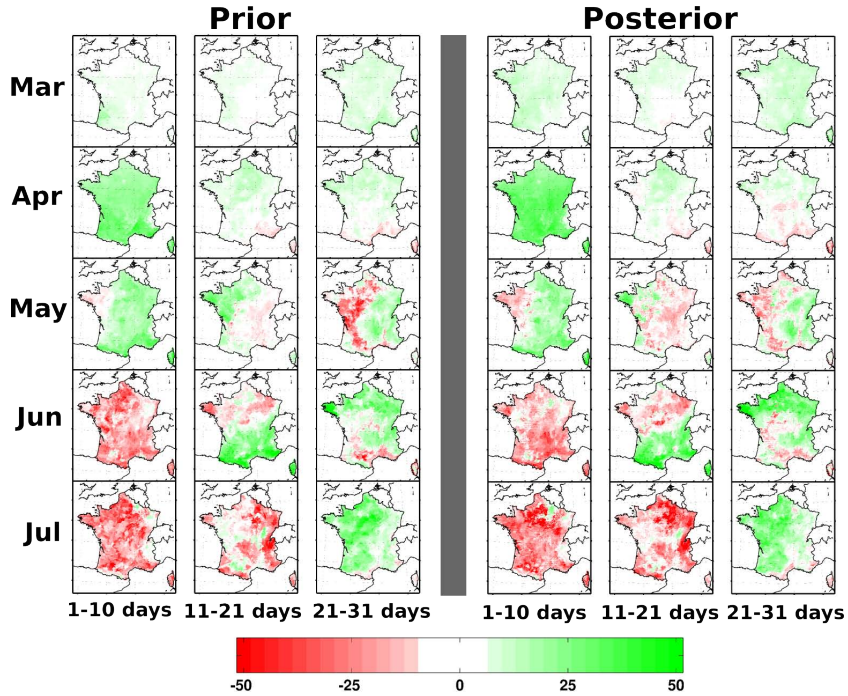

Fig. 12. Change rate calculated over 10 day period for prior and posterior GPP from March to July 2011. The units are in g CO_2 m^{-2} 10 $days^{-1}$.

HESSD
10, 9057–9103, 2013